Bull. Mater. Sci. (2018) 41:45
https://doi.org/10.1007/s12034-018-1549-7

Effect of annealing treatment on optical properties and microstructural variation of $WO_3/Ag/WO_3$ multilayer nano-films

AIDIN HADIFAKOOR, SAEED NIKBIN and GHASSEM KAVEI*
Materials and Energy Research Centre, Tehran 31787-316, Iran
*Author for correspondence (g.kavei@merc.ac.ir, ghassem113@yahoo.com)

MS received 24 March 2017; accepted 30 May 2017; published online 28 March 2018

Abstract. Structural and optical properties of $WO_3/Ag/WO_3$ nano-multilayer composites were investigated for heat mirror applications. $WO_3/Ag/WO_3$ thin films were fabricated through a physical vapour deposition method by using electron-beam evaporation at the vacuum chamber at 10^{-5} Torr. WO_3 nano-layer was fabricated at 40 nm. Annealing treatment was carried out at 100, 200, 300 and 400°C for 1 h after the deposition of first layer of WO_3 on the glass. On WO_3 film, Ag nano-layers with 10, 12 or 14 nm thickness were deposited. Individual layers morphology was investigated using atomic force microscopy (AFM) and deduced that a smoother layer can be achieved after the annealing at 300°C. Ellipsometry analysis was executed to determine both layers, Ag film thickness and inter-diffusion between the WO_3–Ag–WO_3 layers. It was inferred that there was almost no interfering among the WO_3–WO_3 layers in the samples with 12 and 14 nm Ag thickness; while silver was deposited on the annealed WO_3 layer at 300°C. UV–visible spectrophotometer showed that the annealing treatment of the first WO_3 layer enhanced the transparency of films in the visible region. The innovations of the present study have been based on the annealing of the films and finding an optimum thickness for the Ag film at 12–14 nm. Heat mirrors efficiency was assessed according to the principle of their optical behaviour and optimum performance obtained for 14 nm of Ag film, deposited on annealed tungsten oxide at 300°C.

Keywords. $WO_3/Ag/WO_3$; annealing; heat mirror; multilayer; ellipsometry.

1. Introduction

A transparent heat mirror (THM) provides transparency in a visible light in the range of $0.4 < \lambda < 0.7\ \mu m$, while it can reflect IR thermal radiation in the $0.7 < \lambda < 3\ \mu m$ wavelength intervals. THMs have great numbers of applications in many fields, namely energy efficiency, solar photovoltaic conversion and solar heating [1]. Several studies were focused on the heat mirror applications and efficiency [2–4]. A metallic thin film is the main material that is used in fabricating THM due to its high free-electron density, which leads to high reflectance in the visible and infrared ranges [5]. Basically, if the refractive index of the single layer metal film is zero, the most transparency in the visible range can be achieved [6]. In this case, the only loss attributed to the absorption is $4\pi kd/\lambda$, where k is the extinction co-efficient, d is the thin film thickness and λ is the wavelength of the incident light. This reflective loss happens due to the fact that reflectance coefficient of the two interfaces are in opposite phases, which result in destructive interference [7].

There is no perfect metal with $n = 0$, due to undesirable short wavelength absorption reported for the metals like Au and Cu at $\lambda < 0.5\,\mu m$ and at $\lambda \approx 0.8\,\mu m$ for Ag [8], silver with both the lowest refractive index n and absorption in the visible region has been chosen in this study. Nevertheless, when metal is deposited on the dielectric substrates, it experiences a particular process known as growth stages, including metal nuclei, metal islands, large-scale coalescence and a uniform thin film [8]. In the small thickness, a metal film has the propensity for forming an island-like structure, which is regarded as a serious limitation on the heat mirror performance [9]. Furthermore, because of the oxidation and corrosion of a single metal film, it does not present durability and stability required in producing the heat mirrors [10]. Spectrally selective devices can be produced by sandwiching high reflection of metal layers between two dielectric layers [1]. Deposition of uniform layers will produce a great deal of IR reflectivity by dielectric layer surfaces and anti-reflective effect in the visible region. In this case, the dielectric/metal/dielectric (D/M/D) system is able to be more transparent in the visible region and reflective in the IR range. WO_3 films have been widely used in solar energy conversion, storage cells, EC displays, transparent conductors and optical recording and image storage [11]. Hasan *et al* has studied a multilayer system of $WO_3/Ag/WO_3$ to evaluate the intermixing between layers during the deposition of the multilayer coatings for heat mirror applications [12]. However, formation of islands among the layers at the interfaces in the D/M/D systems is a considerable restriction [13]. Effective thickness of silver is reduced when the diffusion process occurs [14]. Sharp interfaces of the layers have a huge impact on heat mirrors efficiency selectivity [15]. In this study, WO_3 thin film

is used as a dielectric layer. Here, we show that annealing treatment of first WO_3 deposited layer has a significant impact on both achieving the effective thickness of the layers and the selectivity of the D/M/D systems.

2. Experimental

$WO_3/Ag/WO_3$ nanoscale multilayer films were deposited by using electron-beam evaporation (Edwards auto 306). The glass substrates were cleaned by ultra-sonication in propanol, followed by acetone and then by de-ionized water for 8 min at each stage; they were dried by exposing them with high purity N_2 gas flow. The source materials were WO_3 powders (Fluka, code 95410) and Ag (Fluka, code 85130, purity 99.99%). WO_3 and Ag films were prepared under vacuum pressure of 10^{-5} Torr. WO_3 or Ag was out-gassed in the vacuum before starting evaporation. The evaporation rates were around 0.1 and 1 nm s^{-1} for WO_3 and Ag, respectively. A quartz crystal thickness monitor controlled the thickness of the layers and the evaporation rate. Furthermore, reliance Stylus profilometer (Taylor Hobson) was used to measure the thickness of the films. Annealing treatment was carried out for WO_3 film at 100, 200, 300 and 400°C for an hour in air. Three different sets of D/M/D systems with different thicknesses of Ag layer at 10, 12 and 14 nm were prepared and characterized. Silver samples A_1, B_1 and C_1 were deposited on annealed WO_3 layer, then WO_3 on top of Ag compared to as-deposited samples A, B and C, respectively. Every set of D/M/D with nominal thicknesses were as follows:

Sample A and A_1: WO_3(40 nm)/Ag(10 nm)/WO_3(40 nm)

Sample B and B_1: WO_3(40 nm)/Ag(12 nm)/WO_3(40 nm)

Sample C and C_1: WO_3(40 nm)/Ag(14 nm)/WO_3(40 nm)

The surface morphology and roughness were examined with atomic force microscopy (AFM) of a Park Scientific instrument applying in non-contact mode. Ellipsometry analysis was carried out for measuring optical constant of the films using Sentech 800 Instrument in different angles. The data analysis was performed using SpectraRay/3 software. Optical transmittance was measured by a UV-visible spectrophotometer (Perkin elmer, Lambda 25 Spectrometer) in the range 300–1100 nm.

2.1 *Models of ellipsometry analysis*

Figure 1 illustrates the models that were employed to represent film characteristics by ellipsometry. WO_3 films can be described by Tauc–Lorentz model (TL), a model applied for modelling dielectric function for both transparent conductive oxides [16] and amorphous materials [17]. TL model uses an empirical relation of the Tauc expression in order of defining the imaginary part of the dielectric function ($\varepsilon_2(E)$) near the band edge and the Lorentz oscillator [18].

Figure 1. Structural models for $WO_3/Ag/WO_3$ thin films on borosilicate glass substrate.

$$\varepsilon_2(E) = A_T \frac{\left(E - E_g\right)^2}{E^2} \Theta\left(E - E_g\right), \tag{1}$$

where $\Theta\left(E - E_g\right)$ is the Heaviside function ($\Theta\,(E < 0) = 0$, $\Theta\,(E \geq 0) = 1$) and E_g is the band gap of material [19]. The real part of the Tauc–Lorentz (ε_1) can be calculated by a Kramers–Kronig integration of $\varepsilon_2(E)$ [20]:

$$\varepsilon_1(E) = \varepsilon_\infty + \frac{2}{\pi} P \int_{E_g}^{\infty} \frac{\xi \varepsilon_2(\xi)}{\xi^2 - E^2} d\xi, \tag{2}$$

where the P indicates the Cauchy principal part of the integral and normally $\varepsilon_\infty = 1$.

Bortchagovsky *et al* [21] proposed that standard Maxwell–Garnett model in the application to the ellipsometry of layers of gold nanoparticles show deficiency. Effective medium approximation (EMA) models require amendment and one of the methods is considered [21]. Diverging to existing 2D models with phenomenological limits, green function approach uses the same number of factors as standard 3D EMA models for explicit calculations of effective parameters of layers of disordered nanoparticles.

For inhomogeneous materials and interfaces between layers, the EMA can be applied to calculate the complex refractive index [22]. Using Bruggeman's EMA equation is common in ellipsometry [23] and it can be written as follows:

$$\sum_{i=1}^{n} f_i \frac{\varepsilon_i - \varepsilon_{eff}}{\varepsilon_i + 2\varepsilon_{ff}} = 0, \quad \sum_{i=1}^{n} f_i = 1, \tag{3}$$

where $n = 2$ indicates two components, and ε_i and f_i are the complex dielectric functions and the volume fraction of the component i, respectively. The mean square error (MSE) between the fitted model and the data was measured

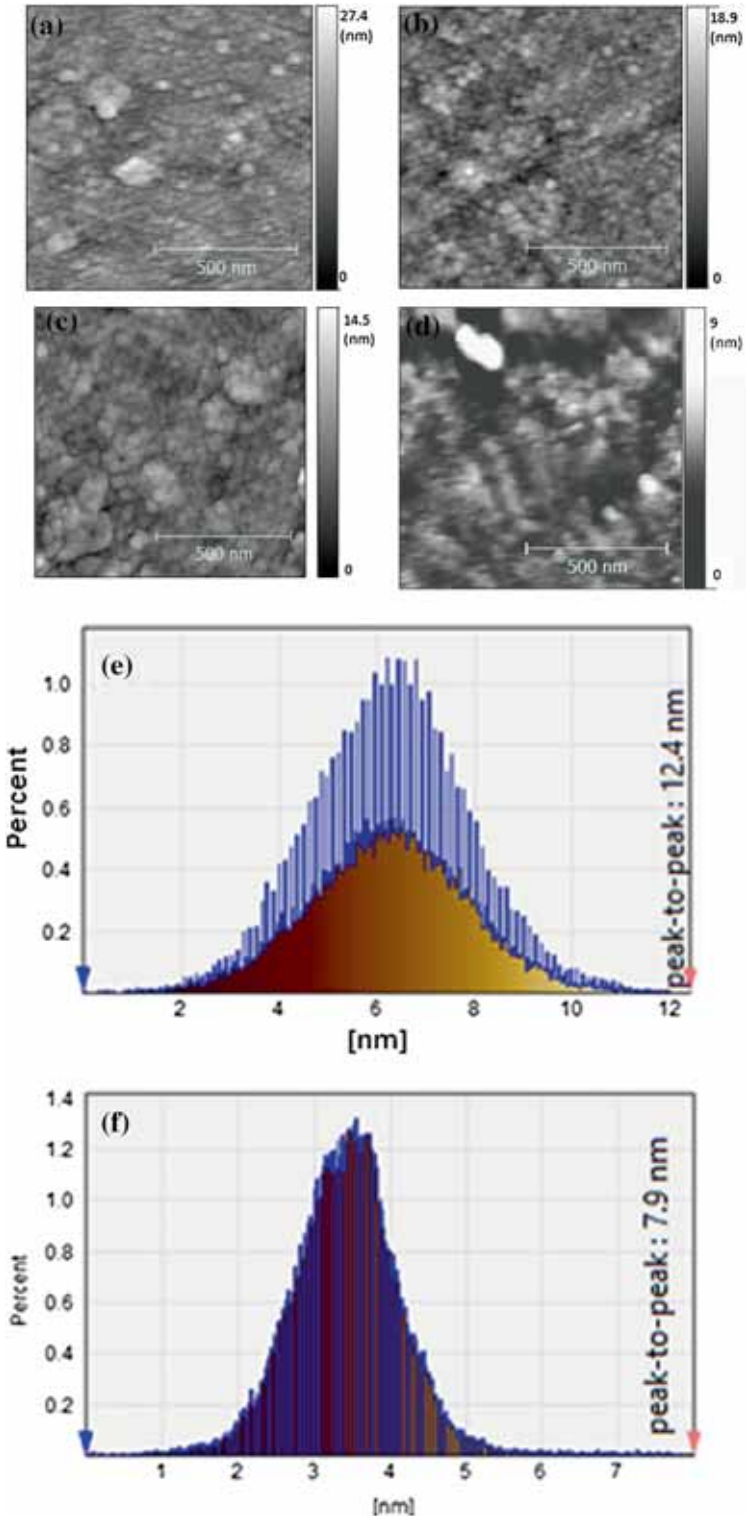

Figure 2. Surface morphology verified by AFM: (**a**) 40 nm tungsten oxide as deposited on the glass; the surface roughness height variation is indicated on the right-hand side trim (0–27.4 nm). (**b–d**) Images of 40 nm tungsten oxide annealed at 100, 200 and 300°C for 1 h, respectively. (**e** and **f**) Images of height distribution of 2D surface–height values from the as-deposited and annealed film at 300°C, respectively.

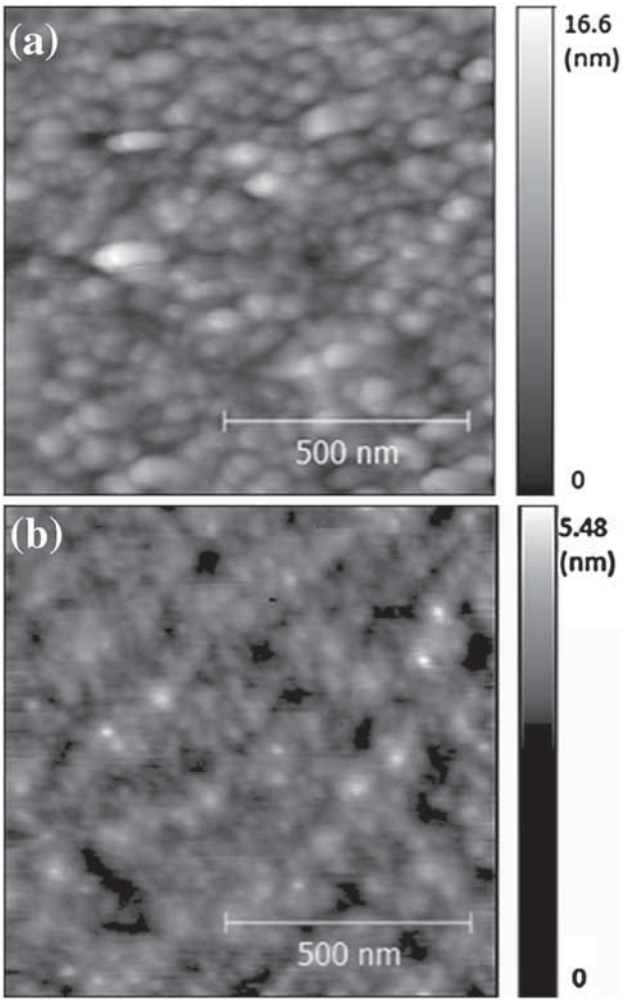

Figure 3. AFM images of the 14 nm Ag films deposited on (**a**) as-deposited tungsten oxide, the surface roughness height variation is indicated on the right-hand side trim (0–27.4 nm and (**b**) annealed tungsten oxide at room temperature.

with Levenberg–Marquardt regression algorithm to assess the goodness of the fit calculated from the measurement data and for analysing the validity of the model employed. This algorithm delivers 90% confidence limit for the fitting data, the better the model corresponds to lower MSE [23].

3. Results and discussion

3.1 *Single films*

Figure 2a displays the AFM image of as-deposited WO_3 thin film, the surface roughness height variation is indicated on the right-hand side trim (0–27.4 nm). While panels b–d demonstrate representative AFM images of WO_3 surfaces annealed at 100, 200 and 300°C. Figure 2 verifies that as-deposited and annealed films at 100 and 200°C have amorphous structures and nanometric grain sizes and these findings are in agreement with other investigations [24]. Syrrokostas *et al* [25] studied WO_3 film's crystal structure after the heat treatment process. XRD patterns of evaporated films show amorphous solids at 300°C. Above this temperature, increment of grain size and large-scale crystallization appeared in AFM at 400°C. The present study reveals above 300°C, it seems that WO_3 films become more 'compact', this was also observed in [26]. A review of the evidence concerning the structural changes of WO_3 by annealing in detail studied in [27].

In order of accomplishing smoother surface, annealing carried out at 300°C for 1 h. Roughness of the WO_3 coated surfaces were 2.5 nm for the as-deposited film and 0.8 nm for annealed film at 300°C that can be seen as the critical decrement. As shown in figure 2e and f, surface–height distribution curves deduced to be narrow in the annealed sample at 300°C compared with the as-deposited one. Peak to peak value decreased sharply from 27.3 nm for as-deposited to 9.1 nm for the film annealed at 300°C. For the film annealed at 400°C, the surface roughness was deteriorated and it affects the transmittance, which is consistent with other previous studies [27].

3.1a *Silver thin films deposited on annealed and as-deposited tungsten oxide layer*: Ag nano-films at 14 nm were deposited on both as-deposited and annealed tungsten oxide layers, simultaneously. Figure 3a and b shows Ag film surfaces from as-deposited and annealed tungsten oxide at 300°C, respectively. The surface roughness height variation is indicated on the right-hand side trim (0–27.4 nm) in figure 3a and (0–5.48) in figure 3b. The figure reveals a lower root mean square (RMS) roughness for annealed film (0.32 nm RMS and 5.1 nm, peak-to-peak surface height distribution) compared with as-deposited (1.9 nm RMS and peak-to-peak = 17 nm). It should be noted that annealing of WO_3 and the parameters of Ag deposition on the film were both crucial in reducing the roughness of Ag and growth of a dense and uniform WO_3 film on the top at room temperature (figure 3b).

3.2 *Ellipsometry analysis*

A precise characterization of the substrates Cauchy model was executed using the borosilicate glass database. The Drude model was designated to represent the Ag thin film. The MSE value was calculated to show the quality of the fitting. Figure 4 shows the measured and best fit ellipsometric data (Ψ, Δ) for various glass/WO_3/Ag/WO_3 thin films for samples A_1, B_1 and C_1. Table 1 demonstrates the thickness of model layers obtained by ellipsometry analysis and the MSE value for each sample.

The extinction coefficient is one of the optical properties that was studied by ellipsometric data. Extinction coefficient is a measure of how strongly a substance absorbs light at a defined wavelength. In the region where the extinction coefficient is zero, there is no absorption. Figure 5a illustrates the extinction coefficient of Ag thin films in 300–900 nm wavelength range calculated by ellipsometry for three different

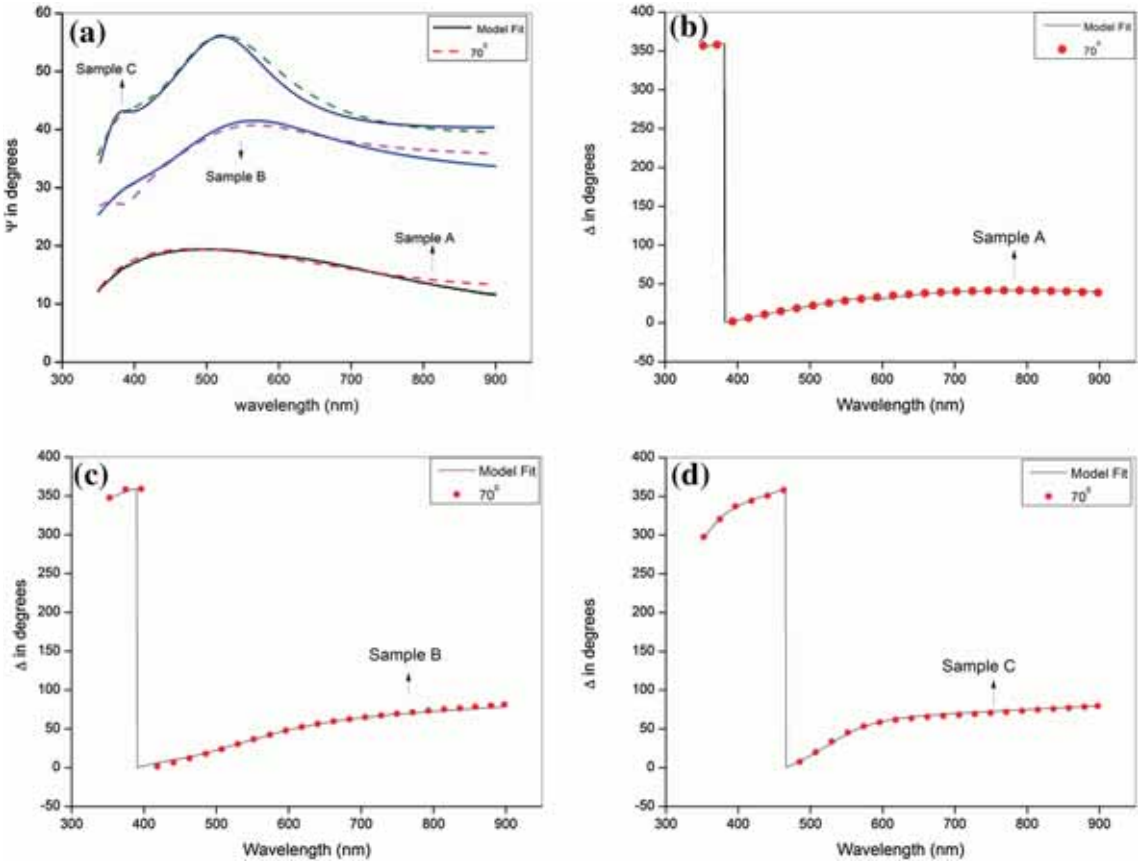

Figure 4. (**a**) Ψ Values for the experiment and model fit for samples A_1, B_1 and C_1. (**b–d**) Δ values for samples A_1, B_1 and C_1, respectively.

Table 1. Thickness and MSE of the layers calculated in ellipsometry.

Model layers	WO_3 (thickness), nm	EMA (thickness), nm	Ag (thickness), nm	EMA (thickness), nm	WO_3 (thickness), nm	MSE
Sample A_1	39.5	7.11	0.86	3.25	37	0.5278
Sample B_1	40.05	0.3	10.9	0.4	39.90	1.2728
Sample C_1	39.80	0.43	13.90	0	40	1.0020

thicknesses, 10, 12 and 14 nm, of the layers that is consistent with previous studies data shown in figure 5b for a typical thickness [28].

Ellipsometry is an indirect measurement for monitoring layer thickness. The complex refractive indices and thickness of the interfaces between layers can be calculated by an EMA theory [29]. Thickness calculated by EMA shows the extent of interference among layers. For this reason, having a uniform layer will result in less inter-diffusion and less EMA thickness. Interfering between the layers can be deduced in sample A1 according to figure 1 and table 1, which can be attributed to the island structure of 10 nm Ag thin film. For samples B1 and C1, EMA thickness decreased significantly due to the uniform structure of Ag thin film. Both, annealing the WO_3 thin film and increasing the thickness of the Ag thin film up to 12 and 14 nm triggers disappearing thin film nucleation and achieve such a uniform film.

3.3 *Optical transmittance*

The optical transmittance spectra of the $WO_3/Ag/WO_3$ multilayer films with different thicknesses of Ag nano-film are being shown in figure 6. Previously we stated that samples A, B and C represent multilayers, which fabricated simultaneously with A_1, B_1 and C_1 samples but annealing was not carried out on their first thin WO_3 film. Owing to the crucial role of silver layer thickness in the heat mirrors performance, figure 6 a silver film with 10 nm thickness did not show the

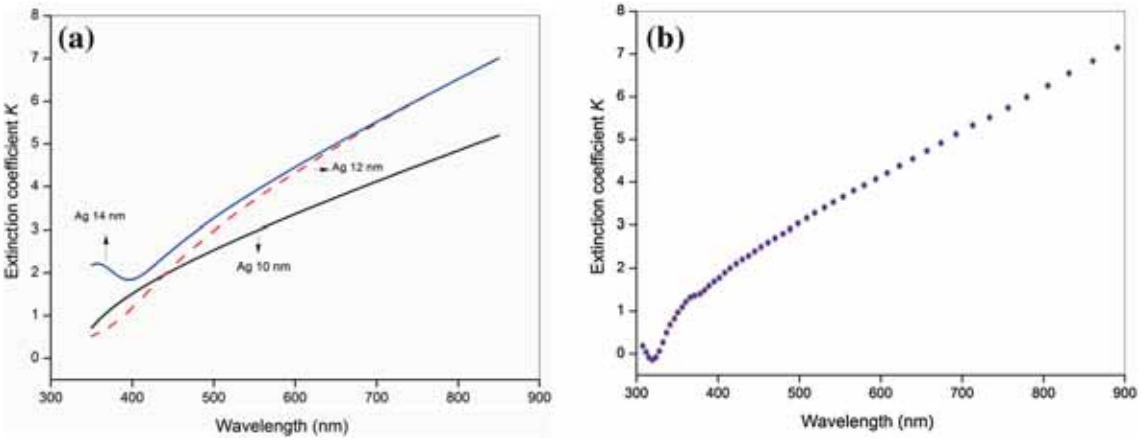

Figure 5. (**a**) Reliance of the extinction coefficient of Ag film on wavelengths for different thicknesses of 10, 12 and 14 nm. (**b**) The extinction coefficient dependency on wavelengths for a typical sample of Ag, obtained by the Filmetrics Company [28].

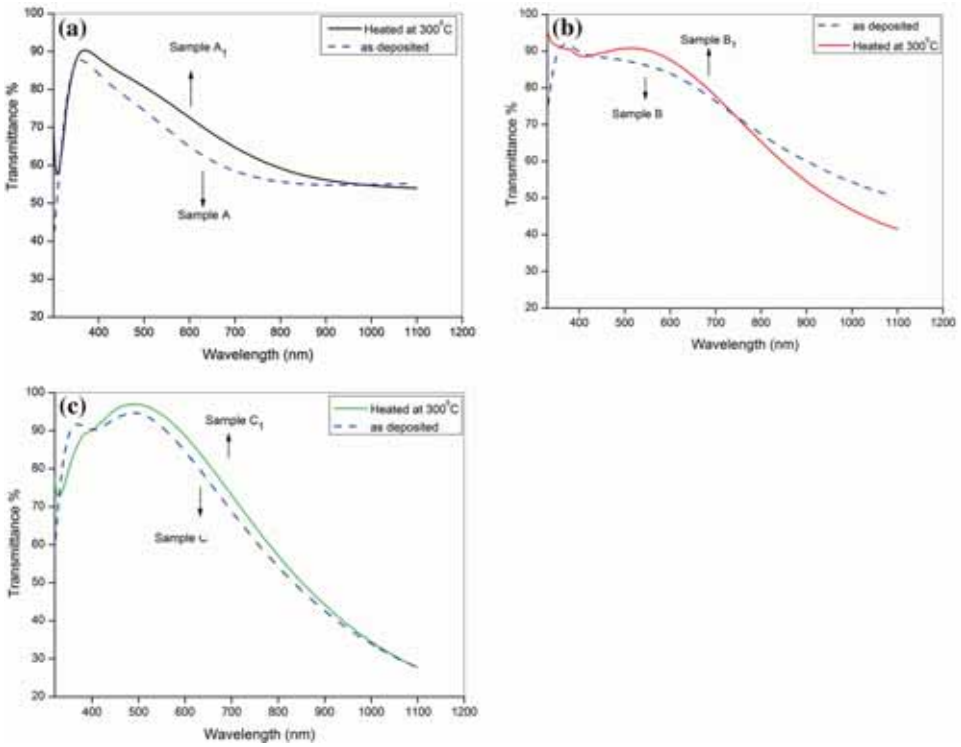

Figure 6. Transmission measured as a function of wavelength in the 300–1100 nm for $WO_3/Ag/WO_3$ thin films deposited on glass. The WO_3 film was fixed at 40 nm and Ag thickness varied (**a**) 10, (**b**) 12 and (**c**) 14 nm.

selectivity, which is needed for the heat mirrors. The failure is attributed to the island and nucleation structure formed in a silver layer, which resulted in an interface among WO_3 layers and scattering the incident light [6]. Optimum silver layer thickness improves the selectivity of D/M/D system. Figure 6b compares the transmittance of two systems with 12 nm of thin silver film thickness, B_1 and B. As it can be seen, the transmittance of W/A/W films is changed from 86% for as-deposited to more than 90% for annealed sample at 300°C. The transmittance decreased significantly to 41.5 and 50% for annealed and as-deposited samples at $\lambda = 1100$ nm, respectively (figure 6b). Figure 6c illustrates transmittance for the sample with 14 nm silver film thickness. W/A/W films transmittance is varied from 91% for as-deposited to more than 94% for annealed one at 300°C in the wavelength of 550 nm, which is one of the highest reported for the

heat mirrors [1,24,30–32]. The transmittance deteriorated dramatically to 27.7 and 27.6% for as-deposited and annealed samples at $\lambda = 1100$ nm, respectively (figure 6c). It is obvious that in addition to Ag thin film thickness; annealing the first WO_3 layer improves transparency in the visible region of light.

4. Conclusion

$WO_3/Ag/WO_3$ heat mirrors were fabricated and the effect of annealing on the first deposited WO_3 film was investigated. Ag thickness varied in the range of 10–14 nm while the thicknesses of WO_3 films were fixed at 40 nm. Multilayer films with a silver thickness of 10 nm did not exhibit the selectivity, which is the main requirement for heat mirrors. The silver film grown on the annealed WO_3 film was considerably smoother and uniform when compared with the Ag film grown on the as-deposited tungsten oxide film. Ellipsometry analysis suggests that there is almost no interference among the WO_3 layers in the samples with 12 and 14 nm of Ag thickness when silver is deposited on the annealed WO_3 layer. Consequently, the effective thickness of the layers increases, which improves the optical performance. The best performance was accomplished for the heat mirror with 14 nm of Ag thickness. For this system, the maximum transmittance at $\lambda = 550$ nm for the annealed sample improved about 3% and reached 94%, which is one of the highest reported for the heat mirrors. It has been concluded that not only annealing forms smooth layers, but also it has a crucial influence on the heat mirrors performance.

Acknowledgements

We would like to acknowledge Dr Mohammad Javad Eshraghi for helpful discussions and support.

References

[1] Fan J C and Bachner F J 1976 *Appl. Opt.* **15** 1012
[2] Selkowitz S 1978 *Presented at the 2nd National Passive Solar Conference, March* 16–18, Philadelphia, PA, p 2. Available from: http://escholarship.org/uc/item/8ss5r1xb
[3] Cai G F, Tu J P, Zhou D, Wang X L and Gu C D 2014 *Sol. Energy Mater. Sol. Cells* **124** 103
[4] Zhou D, Xie D, Shi F, Wang D H, Ge X, Xia X H *et al* 2015 *J. Colloid Interface Sci.* **460** 200
[5] Lampert C M 1981 *Sol. Energy Mater.* **6** 1
[6] Lee C C, Chen S H and Jaing C C 1996 *Appl. Opt.* **35** 5698
[7] Macleod H A 2010 *Thin-film optical filters* 4th ed CRC Press p 209
[8] Granqvist C G 2007 *Sol. Energy Mater. Sol. Cells* **91** 1529
[9] Andersson T and Granqvist C G 1977 *J. Appl. Phys.* **48** 1673
[10] Karlsson B, Valkonen E, Karlsson T and Ribbing C G 1981 *Thin Solid Films* **86** 91
[11] Deb S K 2008 *Sol. Energy Mater. Sol. Cells* **92** 245
[12] Hasan M M, Haseeb A S M A and Masjuki H H 2011 *Surf. Eng.* **27** 382
[13] Al-Kuhaili M F, Al-Aswad A H, Durrani S M A and Bakhtiari I A 2009 *Sol. Energy* **83** 1571
[14] Wang Z, Cai X, Chen Q and Li L 2006 *Vacuum* **80** 438
[15] Fan J C C, Bachner F J, Foley G H and Zavracky P M 1974 *Appl. Phys. Lett.* **25** 693
[16] Fujiwara H and Kondo M 2005 *Phys. Rev. B* **71** 075109
[17] Jellison G and Modine F A 1996 *Appl. Phys. Lett.* **69** 371
[18] www.accurion.com/news/compendium/compendium-dispersion_fun.pdf
[19] www.maths.tcd.ie/~evd/2E2/Notes/Heavisidefunction.pdf
[20] Sancho-Parramon J, Modreanu M, Bosch S and Stchakovsky M 2008 *Thin Solid Films* **516** 7990
[21] Bortchagovsky E G, Dejneka A, Jastrabik L, Lozovski V Z and Mishakova T O 2015 *J. Nanomater.* **2015** 8
[22] Smith G B, Niklasson G A, Svensson J S E M and Granqvist C G 1986 *J. Appl. Phys.* **59** 571
[23] Valyukh I, Green S, Arwin H, Niklasson G A, Wäckelgård E and Granqvist C G 2010 *Sol. Energy Mater. Sol. Cells* **94** 724
[24] Kavei G and Nikbin S 2015 *Mater. Sci.-Poland* **33** 760
[25] Syrrokostas G, Leftheriotis G and Yianoulis P 2015 *Solid State Ion* **277** 11
[26] Wang Z, Chen Q and Cai X 2005 *Appl. Surf. Sci.* **239** 262
[27] Al Mohammad A and Gillet M 2002 *Thin Solid Films* **408** 302
[28] http://www.filmetrics.com/refractive-index-database/Ag/Silver
[29] Bruggemand A G 1935 *Ann. Phys. (Berl.)* **24** 636
[30] Neghabi M, Behjat A, Ghorashi and Salehi S M A 2011 *Thin Solid Films* **519** 5662
[31] Kavei G, Nikbin S and Hadifakoor A 2016 *Int. J. Energy Technol. Policy* **12** 197
[32] Al-Kuhaili M F, Al-Aswad A H, Durrani S M A and Bakhtiari I A 2012 *Sol. Energy* **86** 3183